Electrical Properties and Photoconductivity of Stacked-Graphene Carbon Nanotubes

By *Eduardo. J. H. Lee,* Linjie Zhi, Marko Burghard, Klaus Müllen,* and *Klaus Kern*

Carbon nanotubes (CNTs) and carbon nanofibers (CNFs) have attracted enormous interest in the past years due to their outstanding physical and chemical properties, which render them promising as active elements in novel (opto)-electronic devices.[1,2] While both CNTs and CNFs are carbonaceous materials with a large aspect ratio, their crystalline morphology and, accordingly, their properties are considerably different. In the quasi one-dimensional CNTs, the graphene layer is oriented along the tube axis, and the relative orientation of the honeycomb lattice (i.e., chirality) governs the CNT properties. By contrast, CNFs are comprised of an arrangement of graphitic layers or crystals, which varies with the synthesis procedure, including amorphous and semi-crystalline CNFs,[2–6] whose properties may notably differ. Among the many CNF preparation routes, special attention has been devoted to catalytic plasma-enhanced chemical vapor deposition (PE-CVD). This method yields nanofibers with cone-stacked graphitic morphology and low electrical resistance, which are of interest for interconnect applications.[2–4] More recently, some of us reported a novel type of CNF, wherein the graphene crystallites are stacked perpendicularly with respect to the axis of the nanofiber, forming a tubelike structure.[7,8] The ordered graphitic arrangement of such stacked-graphene carbon nanotubes (SG-CNTs) results from the carbonization of pre-organized columnar superstructures, which are obtained by self-assembly of polycyclic aromatic hydrocarbon (PAH) molecules. However, despite their remarkable morphology, the physical properties of SG-CNTs have not been investigated deeply. Here, we study the temperature-dependent electrical transport properties of individual SG-CNTs in the dark, as well as their electrical response under photoillumination, in order to evaluate their potential for optoelectronic applications.

The synthesis procedure employed for the SG-CNTs has been previously reported.[7] It involves loading of anodic alumina membrane templates with hexa(4-dodecylphenyl)-*peri*-hexabenzocoronene (HBC-PhC_{12}) followed by carbonization, which yields uniformly sized SG-CNTs within the membrane channels. SG-CNT suspensions were obtained by etching the template in an aqueous sodium hydroxide solution, subsequent washing of the final product with water, and dispersion of the SG-CNTs in ethanol using an ultrasonic bath. It is noteworthy that, unlike other CNF synthesis methods, in particular PE-CVD, the present approach does not involve catalysts that may interfere with electrical transport measurements on nanofibers.[9]

In Figure 1a, a bright-field transmission electron microscopy (TEM) image of an individual SG-CNT is displayed. It reveals a hollow, tubelike morphology with a tube-wall thickness of a few tens of nanometers (~20–30 nm) and an outer tube diameter that is approximately ten times larger. High-resolution TEM analysis (Supporting Information) revealed an overall well-ordered stacking despite the presence of slight tilts of the crystal planes occurring in a random distribution along the tubes. Accordingly, the SG-CNTs constitute an assembly of smaller graphene building blocks (see the inset of Fig. 1b), rather than stacks of continuous graphene layers. Raman spectra obtained from individual SG-CNTs ($\lambda_{exc} = 633$ nm, laser power ~500 μW) display two bands, centered on ~1355 cm^{-1} and ~1575 cm^{-1} (cf. Fig. 1b). While the latter band originates from the in-plane vibrations of the two-dimensional graphene crystals (G-band), the former arises due to disorder in the sp^2 lattice (D-band), which, in the present material, is associated with the finite size of the constituting graphene crystallites.[10] By using the empirical Tuinstra–Koenig equation,[10] which relates the D-band/G-band intensity ratio to the size of graphitic crystallites, the lateral dimension of the stacked graphenes is estimated to be of the order of 10 nm.

Electrical devices comprising individual SG-CNTs were fabricated by first depositing the nanotubes on degenerately doped Si substrates with a 200-nm-thick thermally grown oxide layer. Subsequently, gold electrodes (250 nm thickness, 2–6 μm separation, ~1-nm-thick Ti adhesion layer) were defined by electron-beam (e-beam) lithography patterning, followed by metal evaporation and lift-off in *n*-methyl-2- pyrrolidone to remove the residual e-beam resist. A representative atomic force microscopy (AFM) image of such a device is presented in Figure 2a. The measured AFM height of the SG-CNTs (~300 nm) is consistent with their outer diameter determined by TEM. As exemplified by Figure 2b, the room-temperature current–voltage (*I–V*) characteristics of the devices are approximately linear, with two-probe resistances in the range of 100 MΩ–1 GΩ. Four-probe electrical characterization (see the Supporting Information) revealed a negligible contribution of the contacts to the two-probe resistance. Moreover, in measurements using the highly doped Si substrate as back gate, only a weak conductance modulation was observed for gate voltages as high as 20 V (see the Supporting

[*] Dr. E. J. H. Lee, Dr. M. Burghard, Prof. K. Kern
Max Planck Institute for Solid State Research
Heisenbergstrasse 1, 70569 Stuttgart (Germany)
E-mail: e.lee@fkf.mpg.de
Dr. L. Zhi, Prof. K. Müllen
Max Planck Institute for Polymer Research
Ackermannweg 10, 55128 Mainz (Germany)
Dr. L. Zhi
National Center for Nanoscience and Technology of China
Beiyitiao 11, 100190 Beijing (P. R. China)
Prof. K. Kern
Institut de Physique des Nanostructures
Ecole Polytechnique Fédérale de Lausanne
CH-1015 Lausanne (Switzerland)

DOI: 10.1002/adma.200903462

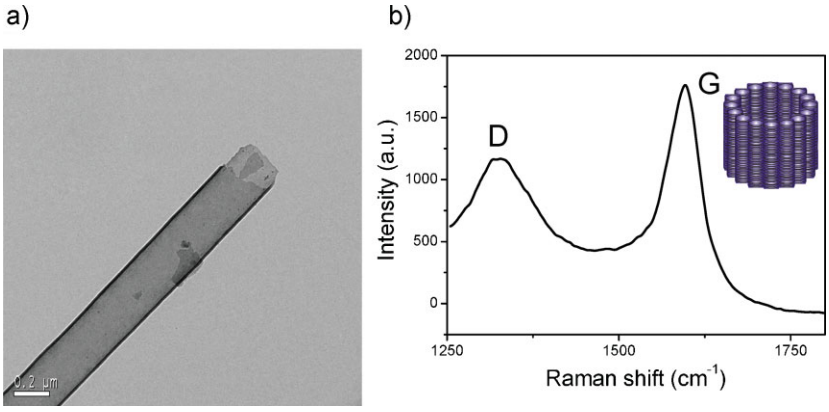

Figure 1. a) Bright-field TEM image of an individual SG-CNT. b) Raman spectrum measured on an individual SG-CNT, with laser excitation at $\lambda = 633$ nm. Inset: illustrative scheme depicting the morphology of a SG-CNT.

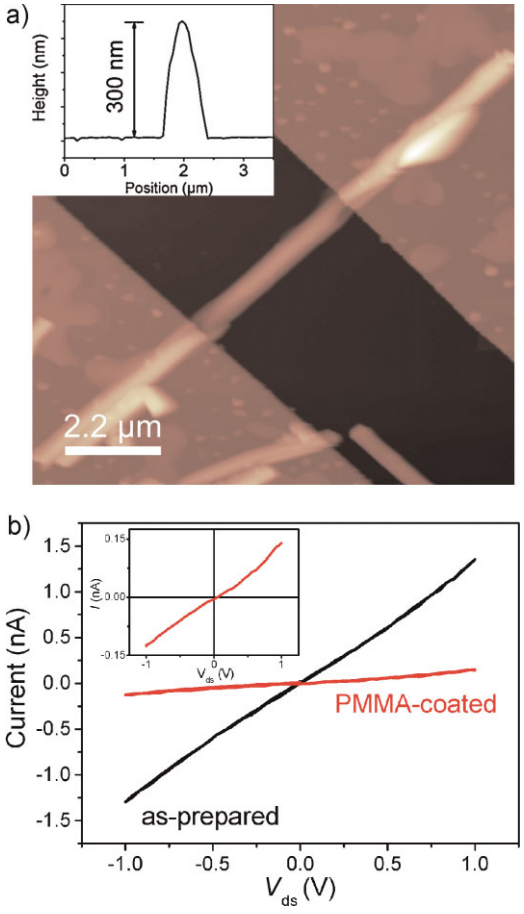

Figure 2. a) AFM image of a device comprising an individual SG-CNT. The measured AFM height (inset) agrees well with the outer-diameter value observed in the TEM micrographs. b) Current–voltage characteristics of a SG-CNT device under ambient conditions (as-prepared, black line) and after being capped in PMMA (PMMA-coated, red line). The inset highlights the electrical response of a PMMA-coated device, whose resistance is approximately one order of magnitude higher than as-prepared devices, resulting from the desorption of doping molecules.

Information). Furthermore, Figure 2b shows that the resistance of individual SG-CNTs increases by approximately one order of magnitude after deposition of a poly(methyl methacrylate) (PMMA) layer and subsequent baking of the sample at 160 °C for 8 h. After removal of the PMMA layer, the device conductance was found to slowly recover under ambient conditions. These observations point towards p-type doping due to oxygen and/or water adsorption from the air in analogy to previous reports on other carbon-based nanomaterials, such as carbon nanotubes and graphene.[11,12]

Based upon the characteristics of the device in Figure 2a (SG-CNT length $L \sim 5$ μm, outer diameter ~300 nm, resistance $R \sim 7$ GΩ under PMMA coating) and assuming an inner tube diameter of 260 nm, a resistivity of $\sim 2.4 \times 10^{-1}$ Ωcm is calculated from $\rho = R \times (A/L)$ (A being the cross sectional area of the tube). Similar values were found for other SG-CNT devices. In general, the resistivity of carbon nanofibers can be described as:

$$\rho(\theta) = \rho_a \sin^2\theta + \rho_c \cos^2\theta \quad (1)$$

where $\rho_a = 4 \times 10^{-5}$ Ω cm and $\rho_c = 4 \times 10^{-2}$ Ω cm are the resistivities of graphite parallel and perpendicular to the basal planes, respectively, and θ is the angle between the graphitic planes with respect to the nanofiber axis.[13] This model describes well the resistivities of PE-CVD grown CNFs, which, due to the cone-stacked morphology of the fibers, fall in an intermediate range between ρ_a and ρ_c (i.e., $\sim 10^{-3}$–10^{-4} Ω cm).[2,13] According to Equation (1), the nanofiber resistivity should assume the value of ρ_c, if the graphitic planes are arranged perpendicularly with respect to the CNF axis ($\theta = 0°$), as is approximately the case in the present samples. Although the resistivity measured in our samples indeed approaches ρ_c it still remains five times larger than the predicted value. This difference reflects the presence of disorder associated with the edges of the graphene crystallites in the SG-CNTs (Fig. 1c), which act as scattering centers for charge carriers passing along the tube axis.

In order to shed further light on the electrical transport mechanism in the SG-CNTs, temperature-dependent electrical measurements were performed. The obtained resistance exhibits an increase by more than two orders of magnitude upon cooling the devices from room temperature to 55 K (Fig. 3). There are three possible mechanisms that may explain the observed temperature dependence: i) thermal excitation of charge carriers across the energy band gap, ii) thermionic carrier injection over contact (Schottky) barriers, and iii) variable range hopping (VRH). Only poor fits resulted when fitting the experimental data to the equations corresponding to mechanisms (i) and (ii) (see the Supporting Information). In contrast, good linear fits were obtained by plotting $\log(I)$ versus $T^{-1/3}$ and $\log(I)$ versus $T^{-1/4}$ (where I and T are current and temperature, respectively), which is suggestive of VRH of charge carriers between localized states.[14] The existence of hopping conduction in the SG-CNTs is

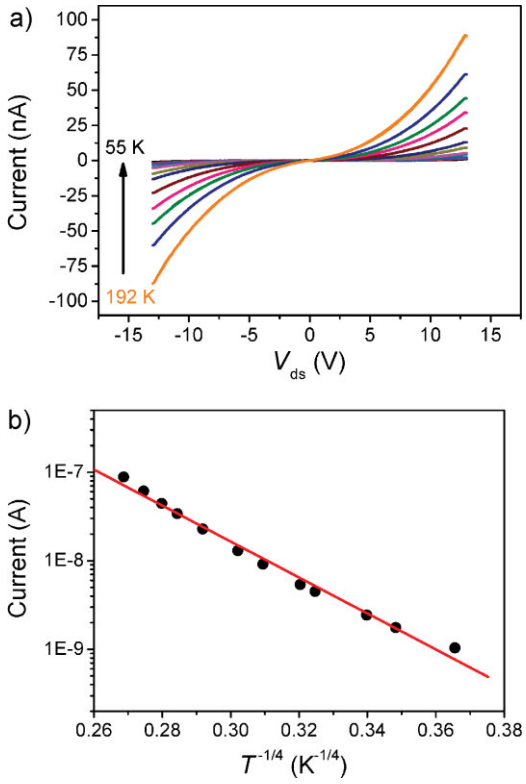

Figure 3. a) Current–voltage characteristics of a SG-CNT device taken as a function of temperature (in the graph, curves acquired between 192 and 55 K are plotted). b) Linear fit of the logarithm of the drain current as a function of $T^{-1/4}$. Such dependence is characteristic of electrical transport by VRH.

consistent with the defective nature of the SG-CNTs stemming from the finite size of the contained graphene crystallites and their imperfect stacking along the tube-axis direction. The temperature dependence of VRH is generally described by $I = I_0 \exp[-(T_0/T)^{1/(d+1)}]$, where the dimensionality of the material d enters the exponent. The good quality of the fit to the $T^{-1/4}$ dependence hints toward an effective three-dimensional hopping between the graphene crystallites in SG-CNTs (Fig. 3b). However, it should be emphasized that electrical data over a broader temperature range would be required to conclusively distinguish between two- and three-dimensional hopping.

Finally, the photoconductivity of individual SG-CNTs was examined under ambient conditions using a confocal laser microscope. Global illumination of the SG-CNTs with $\lambda = 633$ nm caused a pronounced current increase over the entire bias range (Fig. 4a). The drain current through an as-prepared and a PMMA-coated SG-CNT device as the laser illumination was switched on and off is depicted in Figure 4b. As a common feature of both samples, the photoirradiation leads to an instantaneous current increase. However, the bare device is distinguished from the PMMA-coated one in that after switching off the light it shows an enhanced resistance, which only slowly recovers over a time scale of minutes to the original value before illumination. Similar resistance increases upon photoirradiation have been observed in carbon nanotube transistors, for which they were attributed to photodesorption of oxygen.[15] On the

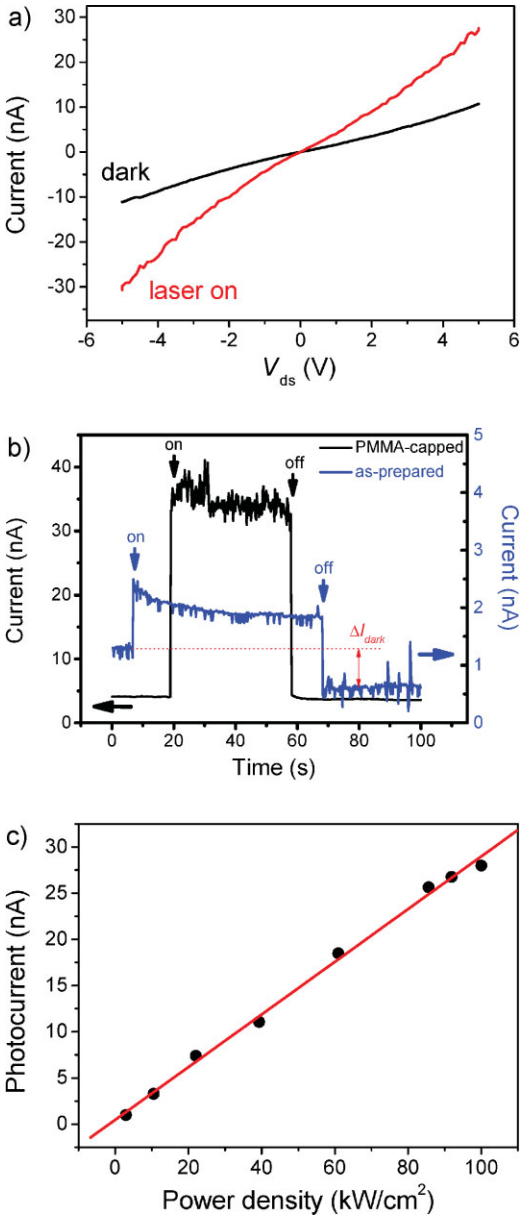

Figure 4. a) Current–voltage characteristics of a SG-CNT device measured in the dark (black line) and under 633-nm laser irradiation (red line). b) Changes observed in the drain current of as-prepared (blue line, measured with $V_{ds} = 1$ V) and PMMA-capped (black line, measured with $V_{ds} = 5$ V) devices upon manually chopping the photoillumination. The data points between the "on" and "off" labels correspond to the period when the laser was incident on the samples. c) Magnitude of the photocurrent response as a function of the laser power density.

basis of the aforementioned effect of air exposure on the electrical properties of the SG-CNT devices (Fig. 2a), the same explanation is likely to hold for the present observations. In addition, a linear relationship was observed between the magnitude of the photocurrent (I_{pc}), i.e. the increment in the drain current induced by photoexcitation and the laser power density (Fig. 4c), as expected for photoconductivity processes. Toward assessing the potential of the SG-CNTs for photodetection applications, we have estimated their responsivity $R_{rs} = I_{pc}/P \cdot A_{eff}$ as a figure of

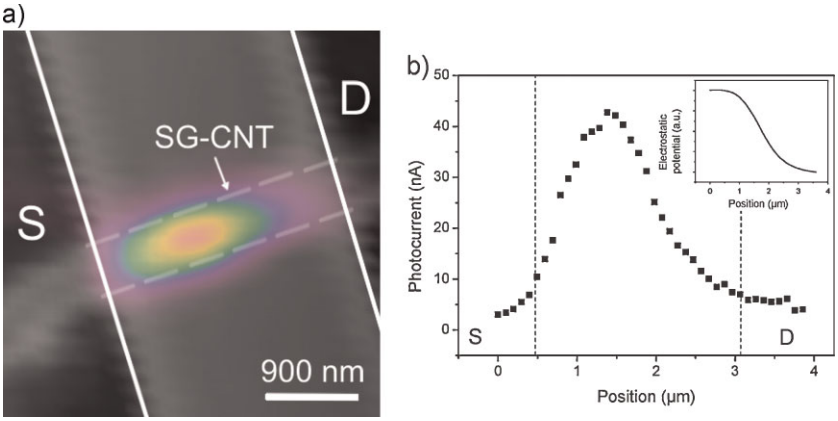

Figure 5. a) SPCM image of a SG-CNT device, taken under ambient conditions with $V_{ds} = 5$ V. The photocurrent signal is plotted in a false-color scale and the optical-reflection image is superimposed in gray scale. S and D corresponds to the source and drain contacts, respectively. b) Line profile of the photocurrent response taken from the source to the drain contacts. The two vertical dashed lines mark the edges of the source and drain contact. The inset schematically depicts the electrostatic potential distribution within the SG-CNT device, as obtained by integrating the photocurrent profile.

merit for the photocurrent-generation efficiency, where P corresponds to the laser power density and A_{eff} is the effective device area. For the investigated PMMA-coated devices with $P = 100\,\mathrm{kW\,cm^{-2}}$, $I_{pc} = 30$ nA at 5 V bias, and A_{eff} equivalent to the outer diameter of the SG-CNT multiplied by its length ($A = 2\,\mu\mathrm{m} \times 300$ nm), a responsivity of $\sim 0.05\,\mathrm{mA\,W^{-1}}$ is obtained. This value is one order of magnitude lower than that reported for single-ZnO-nanowire devices at 1 V bias ($R_{rs} \sim 0.5\,\mathrm{mA\ W^{-1}}$).[16] The responsivity is also inferior to single-polymer-nanowire photodetectors ($R_{rs} \sim 0.4\,\mathrm{mA\ W^{-1}}$),[17] albeit in this case it was derived at much higher applied bias (40 V).

In order to explore the photocurrent-generation mechanism in the SG-CNTs, scanning photocurrent microscopy (SPCM) measurements were performed. In this technique, spatially resolved photocurrent maps are recorded using a diffraction-limited laser spot as the excitation source.[18,19] Figure 5a displays a photocurrent image of an individual contacted SG-CNT acquired with $V_{ds} = 5$ V ($\lambda = 633$ nm and $P = 100\,\mathrm{kW\ cm^{-2}}$). The image reveals a non-homogeneous signal distribution along the tube, with a photocurrent maximum located in vicinity of the source contact and an asymmetric, exponential decay towards the electrical contacts (Fig. 5b**)**. Other SG-CNTs exhibited essentially the same response. Similar photoresponses have been reported for CdS nanowire devices with Ohmic contacts,[19] whereas it is well-distinguished from CNTs, wherein the photocurrent response is strongly dominated by the electrical contacts due to the presence of Schottky barriers.[18] In the former case, the SPCM signals were explained by the diffusion of photoexcited carriers to the electrodes limiting the photoconductivity. However, this mechanism is not able to describe the photoresponse of SG-CNT devices, as apparent from the mostly unchanged photocurrent distribution observed upon inverting drain and source contacts (see the Supporting Information). Hence, it is concluded that the signal pattern reflects the local electric-field distribution within the SG-CNT devices, thus providing access to electrostatic potential profiles by integrating the photocurrent response (see the Supporting Information).[18] These profiles indicate a potential drop along the nanofiber (inset in Fig. 5b), demonstrating that the detected photoconductivity indeed stems from the "body" of the SG-CNTs.

In summary, the electrical resistivity of individual, stacked-graphene carbon nanotubes has been found to be nearly five times larger than for graphite crystals perpendicular to their basal planes. This difference is attributable to the granular morphology of the SG-CNTs, specifically the disorder at the edges of the constituting graphene islands causing enhanced carrier scattering. The inherent disorder is furthermore manifested in the occurrence of hopping conducting in this nanostructured carbon material. Moreover, the SG-CNTs have been demonstrated to be moderate photoconductors. One possible strategy to improve the responsivity of SG-CNTs may be sensitization with appropriate dye molecules.

Acknowledgements

The authors thank Adarsh S. Sagar for performing the Raman spectroscopy measurements. L.Z. and K.M. acknowledge financial support by the Max-Planck Society through the ENERCHEM program. Supporting Information is available online from Wiley InterScience or from the author.

Received: October 8, 2009
Published online: February 26, 2010

[1] "*Carbon Nanotubes: Synthesis, Structure, Properties and Applications*", (Eds: M. S. Dresselhaus, G. Dresselhaus, Ph. Avouris) Springer Verlag, Heidelberg, Germany **2001**.
[2] A. V. Melechko, V. I. Merkulov, T. E. McKnight, M. A. Guillorn, K. L. Klein, D. H. Lowndes, M. L. Simpsons, *J. Appl. Phys.* **2005**, *97*, 041301.
[3] Y. Chen, L. P. Guo, D. J. Johnson, R. H. Prince, *J. Cryst. Growth* **1998**, *193*, 342.
[4] J. C. Coiffic, D. Mariolle, N. Chevalier, S. Olivier, D. Lafond, M. Fayolle, S. Maitrejean, H. Le Poche, *Appl. Phys. Lett.* **2008**, *92*, 223510.
[5] N. Jiang, R. Koie, T. Inaoka, Y. Shintani, K. Nishimura, A. Hiraki, *Appl. Phys. Lett.* **2002**, *81*, 526.
[6] S. C. Suen, W. T. Whang, B. W. Wu, Y. F. Lai, *Appl. Phys. Lett.* **2004**, *84*, 3157.
[7] L. Zhi, J. Wu, J. Li, U. Kolb, K. Müllen, *Angew. Chem. Int. Ed.* **2005**, *44*, 2120.
[8] L. Zhi, T. Gorelik, J. Wu, U. Kolb, K. Müllen, *J. Am. Chem. Soc.* **2005**, *127*, 12792.
[9] Y. Ominami, Q. Ngo, M. Suzuki, A. J. Austin, C. Y. Yang, A. M. Cassell, J. Li, *Appl. Phys. Lett.* **2006**, *89*, 263114.
[10] F. Tuinstra, J. L. Koenig, *J. Chem. Phys.* **1970**, *53*, 1126.
[11] P. G. Collins, K. Bradley, M. Ishigami, A. Zettl, *Science* **2000**, *287*, 1801.
[12] F. Schedin, A. K. Geim, S. V. Morozov, E. W. Hill, P. Blake, M. I. Katsnelson, K. S. Novoselov, *Nat. Mater.* **2007**, *6*, 652.
[13] L. Zhang, D. Austin, V. I. Merkulov, A. V. Meleshko, M. A. Guillorn, D. H. Lowndes, M. L. Simpsons, *Appl. Phys. Lett.* **2004**, *84*, 3972.
[14] H. Böttger, V. V. Bryksin, *Hopping Conduction in Solids*, VCH, Berlin, **1985**.
[15] R. J. Chen, N. R. Franklin, J. Kong, J. Cao, T. W. Tombler, Y. Zhang, H. Dai, *Appl. Phys. Lett.* **2001**, *79*, 2258.
[16] H. Kind, H. Yan, B. Messer, M. Law, P. Yang, *Adv. Mater.* **2002**, *14*, 158.
[17] G. A. O'Brien, A. J. Quinn, D. A. Tanner, G. Redmond, *Adv. Mater.* **2006**, *18*, 2379.
[18] E. J. H. Lee, K. Balasubramanian, J. Dorfmueller, R. Vogelgesang, N. Fu, A. Mews, M. Burghard, K. Kern, *Small* **2007**, *3*, 2038.
[19] Y. Gu, J. P. Romankiewicz, J. K. David, J. L. Lensch, L. J. Lauhon, *Nano Lett.* **2006**, *6*, 948.